Optic Disc segmentation based on level-set and colour gradients

Aurora Sáez*, Irene Fondón*, Begoña Acha*, Soledad Jiménez**, Pedro Alemany, Qaisar Abbas****, Carmen Serrano*;***
***Departamento de Teoría de la Señal y Comunicaciones. Universidad de Sevilla, Spain; **Hospital Universitario Puerta del Mar, Cádiz, Spain; ***Surgery Department, University of Cádiz, Cádiz, Spain; ****Department of computer Science, National Textile University, Faisalabad, Pakistan**

Abstract

Optic Disc (OD) segmentation is a key preprocessing component in many algorithms designed for the automatic extraction of retinal anatomical structures and lesions , thus, an associated module of most retinopathy screening systems. Most of the OD segmentation algorithms processes exclusively one colour plane of the retinography, thus discarding colour information. In this paper, a new algorithm for the segmentation of the OD is proposed. After a pre-processing step to remove vessels, an edge-based level-set algorithm is applied. The main contribution of the paper consists in the utilization of the colour information during the segmentation. Specifically, vector gradients in $L^*a^*b^*$ are applied in the edge-based level-set algorithm and, instead of the Euclidean norm, CIE94 colour difference formula is applied to those vector gradients. In addition, in the vessel removal step, the three-plane image is modified in $L^*a^*b^*$ colour space. The proposed algorithm was tested with 22 retinographies where physicians had manually detected OD edges. The algorithm was able to automatically detect the OD in all the cases, with a 92,35% of intersection between the OD area marked by physicians and the OD detected with the algorithm. The Mean Distance to the Closest Point was also calculated and it was under 5 pixels for 100% of the images.

Introduction

Potentially blinding eye conditions such as AMD (Age-related macular degeneration), DR (Diabetic retinopathy) and glaucoma are increasing as the number of people affected grows. Three-quarters of all blindness cases can be prevented or treated especially when they are early detected through regular screening [1]. Early detection screenings consist primarily of obtaining fundus images through photography. However, with a large number of patients undergoing regular screenings, tremendous amount of time is needed for the medical professionals to analize and diagnose the fundus photographs. As a result, the patients are referred to ophthalmologist for further examination and treatment. Therefore, by automating the initial task of analyzing the huge amount of retinal photographs for symptoms of diseases, the efficiency of the screening process can be greatly improved.

The optic disc (OD) is considered one of the main features of a retinal fundus image. OD detection is a key preprocessing component in many algorithms designed for the automatic extraction of retinal anatomical structures and lesions , thus, an associated module of most retinopathy screening systems [2]. The OD often serves as a landmark for other fundus features. As a first example, as there exists an approximately constant distant between OD and the fovea, OD location can be used as a priori knowledge to help estimating the location of the macula [3]. Secondly, the OD was also used as an initial point for retinal vasculature detection methods; large vessels can be found in the OD neighborhood and they can be utilized as seeds for vessel tracking methods [3]. Thirdly, the change in the shape, colour or depth of OD is an indicator of various ophthalmic pathologies especially for glaucoma [4]. On the other hand, in Computer Aided Diagnosis tools for early diagnosis of diabetic retinopathies, the OD can initially be recognized as candidate exudates regions in methods to automatically detect exudates [5]. Thus, if the OD is detected and removed the classification rate of exudate regions is improved.

Although the OD has well-defined features and characteristics, localizing the OD automatically and in a robust manner is not a straight-forward process, since the appearance of the OD may vary significantly due to retinal pathologies. Consequently, in order to effectively detect the OD, the various methods developed should consider the variations in appearance, size, and location among different images. Thus, numerous methods to detect the optic disc appear in the literature. But many of them utilized only part of the colour information contained in the image, such as one colour plane [2, 6, 7, 8].

In this paper we proposed to process each colour pixel as a colour vector. Firstly, in the vessel removal step, the image is modified in $L^*a^*b^*$ colour space. In the same way, a vector gradient is used during the level-set procedure. In addition, we utilize an uniform colour space, 1976 $L^*a^*b^*$, and we replace the Euclidean distance with the colour distance $CIE94$ in the vector gradient. Despite the fact that the CIEDE2000 equation is more recent and performs better than CIE94 for some data sets, its added complexity is probably not justified for most practical applications [9]. In this paper, both equations were tested experimentally. The high computational cost of the CIEDE2000 computation did not justify its use, as similar results were obtained with both equations.

Methodology

In this section the methodology used is presented. The data flow diagram in Fig. 1 gives an overview of the main steps. First, a method to remove the blood vessels present in the image was implemented. To segment the optic disc a level set formulation was applied to a colour gradient. This vector gradient was implemented in CIE $L^*a^*b^*$ colour space and used CIE94 distance formula. As a initial curve is required for the level set formulation, optic disc localization and ROI definition were needed. The initial curve was defined by this ROI. In this paper, the retinal images are supposed sRGB under the illuminant D65, since the acquisition system is unknown.

Blood vessels removal

The identification and removal of the vascular structure is a necessary prerequisite to obtain the OD area. In the proposed approach we have utilized the algorithm designed for hairs suppression in melanoma images presented by Qaisar et al. [10]. As blood vessels are lines of a certain width, the procedure of restoring the information occluded by hair lines could be applied to blood vessels achieving accurate results. The proposed blood

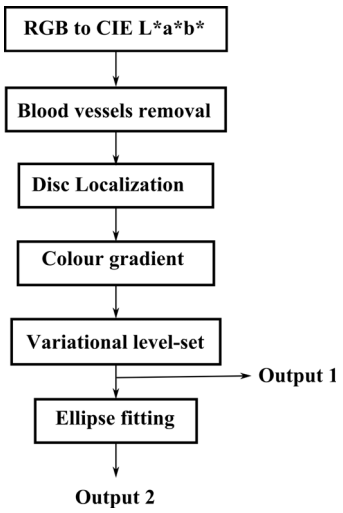

Figure 1. *Proposed system*

vessels removal algorithm is divided into three steps: vessels detection with the use of the derivative of a Gaussian (DOG)[11], refinement of the obtained result with morphological techniques and vessels substitution by fast marching image inpainting [12] technique.

Disc Localization

The optic disc can be identified as a bright region on a retinal fundus image [13]. Therefore, lightness information was used to detect the disc localization. The channel L^* of $L^*a^*b^*$ colour space was smoothed by an averaging filter. The pixels of the result image with intensity value higher than 97% of the maximum intensity value were selected. The mass centre of this set of pixels was calculated. A square with radius of 90 pixels and centred at that mass center was used to determine the ROI. This square defined the initial contour required for the level-set segmentation, explained in a following section.

Colour gradient

The edge-based level set methods are applied to a gradient image. In the literature, all of the authors use the gradient of a single channel in the problem at hand, example of that is the work of Wong et al. [14], where the level-set algorithm was applied to the red channel. However, in this paper the colour information was taken into account, and a colour gradient was used [15].

In colour gradients, the vector nature of colour is preserved throughout the computation. Colour images can be viewed as a two-dimensional three channel vector field. Each pixel in this vector field is characterized by a discrete integer function $\mathbf{a}(x,y)$. The value of this function at each point is defined by a three dimensional vector in a given colour space. Therefore, a pixel is defined as:

$$\mathbf{a}(x,y) = \begin{bmatrix} C_1(x,y) \\ C_2(x,y) \\ C_3(x,y) \end{bmatrix} \tag{1}$$

where $C_i(x,y)$ represents the value of the pixel in the i-th colour plane ($i = 1,2,3$), and (x,y) refers to the spatial dimensions in the 2-D plane.

The operator Sobel based on the first derivative, commonly applied in grayscale imaging, can be generalized into the multi-dimensional [16]. In this paper, Sobel mask was applied to CIE

$\mathbf{a}_1$	$\mathbf{a}_2$	$\mathbf{a}_3$
$\mathbf{a}_4$	$\mathbf{a}_5$	$\mathbf{a}_6$
$\mathbf{a}_7$	$\mathbf{a}_8$	$\mathbf{a}_9$

Figure 2. *Sliding window*

$L^*a^*b^*$ image by constructing the vectors (according to the notation used in Fig. 2): $V_1^+ = a_3 + 2a_6 + a_9$, $V_1^- = a_1 + 2a_4 + a_7$, $H_1^+ = a_7 + 2a_8 + a_9$, $H_1^- = a_1 + 2a_2 + a_3$. The gradient along x and y direction respectively, is shown in equation 2 and 3.

$$VD_x = \triangle E\left(V_1^+, V_1^-\right) \tag{2}$$

$$VD_y = \triangle E\left(H_2^+, H_2^-\right) \tag{3}$$

where $\triangle E$ denotes the CIE94 colour difference between the two vectors defined in the CIE $L^*a^*b^*$ colour space. Usually, the Euclidian distance (CIELAB) is used for this purpose, however the CIE94 colour distance was used in this paper because it has been shown that CIE94 outperforms CIELAB [15].

The gradient magnitude is computed as shown in equation 4.

$$VD = \sqrt{VD_x^2 + VD_y^2} \tag{4}$$

Variational level-set

Once blood vessels are removed, optic disc segmentation is carried out by using a variational level set formulation.

Level set methods, which were first introduced by Osher and Sethian [17], have been widely used as global approaches optimizing active contours for the segmentation of objects of interest from the background [18] [19] [20]. The basic idea is to represent contours as the zero level set of an implicit function defined in a higher dimension, usually referred as the *level set function* ($\phi(t)$). The challenge of a level-set algorithm is to make (ϕ) evolve so that its zero level converges at the real boundaries in the image.

The general level set equation is presented in 5,

$$\frac{\partial \phi}{\partial t} + F|\nabla \phi| = 0 \tag{5}$$

where F represents the speed function and ϕ the level set function. One of the main challenges in the employment of level set techniques has been the generation of shocks which can result in less than accurate contours. To overcome this, the method developed by Li et al [21] is employed. In the reported work, an energy function ε is introduced into (5) to maintain the level set function near the signed distance function, thus avoiding the need for re-initialization of the level set function. It has been shown that the resulting expression is the following gradient flow:

$$\frac{\partial \phi}{\partial t} = \mu\left[\triangle\phi - div\left(\frac{\nabla\phi}{|\nabla\phi|}\right)\right] + \lambda\delta(\phi)div\left(g\frac{\nabla\phi}{|\nabla\phi|}\right) + \nu g\delta(\phi) \tag{6}$$

where μ determines the deviation of ϕ from a signed distance function, λ and ν are the coefficients of the weighted length of the zero level curve and of the weighted area inside the zero level curve respectively, and t is the time step of the experiment.

The second and the third term in the right hand side of (6) are responsible of driving the zero level curve towards the object boundaries. g is the edge indicator function defined by:

$$g = \frac{1}{1 + |\nabla G_\sigma * I|^2} \tag{7}$$

where G_σ is the Gaussian kernel with standard deviation σ, I is the test image and $*$ is the convolutional operator.

In this paper, the gradient used in this definition was the vector gradient explained in the previous section. Therefore, the g definition is modified as:

$$g = \frac{1}{1 + (VD(G_\sigma * I))^2} \tag{8}$$

where VD is the vector gradient magnitude implemented in CIE $L^*a^*b^*$ using CIE94 colour difference equation, explained in the previous section.

Ellipse fitting

The output of the above step is the contour of the optic disc. However, several authors [14], [23] used a ellipse fit as post-processing step in order to smooth this detected contour. In this paper, the results obtained with and without ellipse fitting were studied.

Results and Evaluation

Some results of the proposed method can be seen in Fig. 3 and Fig. 4, where a) shows the original image, b) image without the bool vessels, c) manually segmented optic disc in green and segmented by the proposed method in blue d) ellipse fitting to contour manually segmented (green) and to the contour detected (blue). Both results, output of the level set and output of the ellipse fitting, were evaluated.

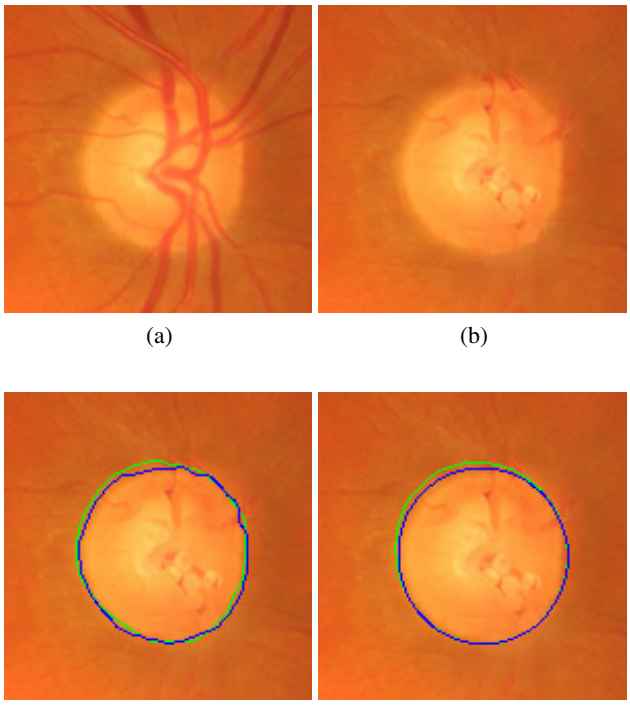

Figure 3. *a) original image, b) bool vessels removal, c) optic disc manual segmentation (green) and segmentation by the level set (blue) d) ellipse fitting to contour manually segmented (green) and to the detected contour (blue).*

The method was tested with 22 images manually segmented by experts from Hospital Puerta del Mar, Cádiz, Spain to evaluate its performance. Two measurements were analysed. The first

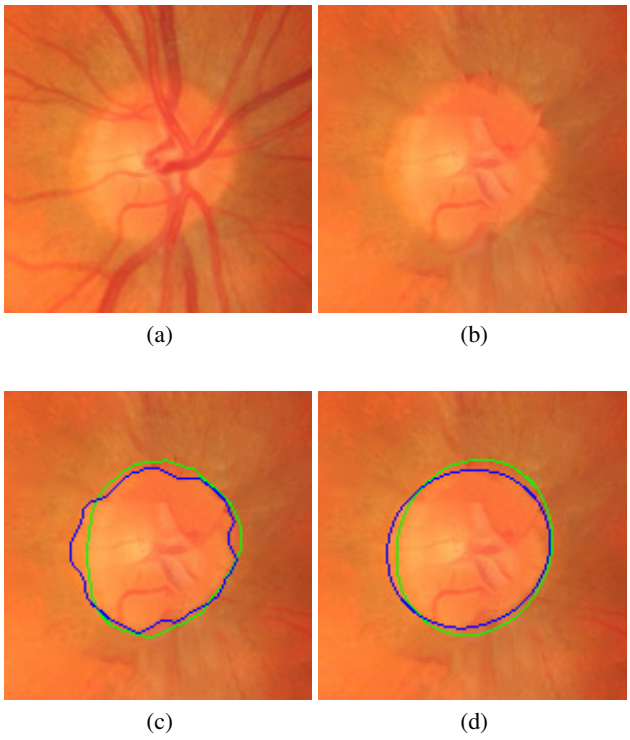

Figure 4. *a) original image, b) bool vessels removal, c) optic disc segmentation manually (green) and segmentation by the level set (blue) d) ellipse fitting to contour manually segmented (green) and to the contour detected (blue).*

one compares intersection of areas delimited by manual and automated segmentation. The second measurement gives an idea of the contours deviation.

For comparing the intersection of the areas, the enclosed areas of both contour lines (manual and automated segmentation) were compared pixel by pixel. As a reference area for each image, the area delimited by the manually outlined contour was used. The success percentage was defined as the percentage of the size of the reference area intersection with the area segmented by the method. False positive (FP) rate was defined as the area erroneously segmented as optic disc by the method. And false negative (FN) rate as the area belonging to disc optic that it has not been segmented by the method. These definitions are clearly represented in Fig. 5. In Table 1 the results with and without ellipse fitting are shown. Chrastek et al. [24] used this method to evaluate their proposed segmentation algorithm in 159 images, which included glaucomatous and normal subjects. The results are shown in table 1. This database of images is not in public domain.

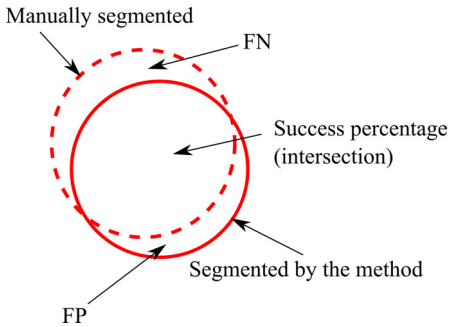

Figure 5. *Intersection of the areas*

Table I. Results of intersection of the areas

Method	% success percentage	% FN	% FP
With ellipse fitting	92.35%	7.64%	4.7%
Without ellipse fitting	92.32%	7.67%	5.67%
Chrastek et al. [24]	91%	9%	10%

Table II. Mean distance to closest point (MDCP)

Method	With ellipse fitting	Without ellipse fitting
MDCP	2.72 pixels	3.07 pixels
$MDCP < 3$ pixels (% images)	66.66%	59.09%
$3 \leq MDCP \leq 5$ pixels (% images)	33.33%	36.36%
$MDCP > 5$ pixels (% images)	0%	4.54%

The second measurement, called mean distance to the closest point (MDCP) [25], evaluates the average distance from the detected boundary to the ground truth. Ground truth is the contour of the reference area (manually segmented area). Reference contour, denoted by R, consists of the individual pixels r_i, $i : 1,2,...,M$, where M is the amount of the pixels on the reference contour. S is the final contour detected by the proposed method. For each contour point $S(n)$ $n : 1,2,...,N$, the distance to the closest point (DCP) of reference contour is defined as:

$$DCP(S(n),R) = min\|S(n) - r_i\|, \;\; i : 1,2,...,M \tag{9}$$

The accuracy of the detected boundary is evaluated by the mean of DCP (MDCP) as follows:

$$MDCP(S,R) = \frac{1}{N}\sum_{n=1}^{N} DCP(S(n),R) \tag{10}$$

The result obtained with MDCP are summarized in Table 2. The measured MDCPs are, respectively, 2.72 and 3.07 pixels for the proposed method with ellipse fitting and without it. In the table is also shown percentage of images obtained with $MDCP <$ 3 pixels, with $3 \leq MDCP \leq 5$ pixels and with $MDCP > 5$ pixels for both outputs.

Discussion and conclusions

OD detection is an important preprocessing step in Computer Aided Diagnosis(CAD) systems for many retinopathies. Specifically, in glaucoma diagnosis an important parameter is cup-optic disc ratio (CDR). Therefore, a strong effort has been directed toward an accurate OD segmentation. Nevertheless, notwithstanding that retinographies are colour images, most of the improvements in OD segmentation have been applied to one colour plane [2, 6, 7, 8]. In [7, 2, 6], good OD location rates are reported but the precise OD edges are not estimated. [8] presents a sensitivity of 0.86. In this paper, a new method that locates the OD edges has been presented. It obtains a high sensitivity (92.35%) in the edge estimation. Probably this improvement in comparison with [8] is due to the use of the colour information contained in the image: vessel removal is performed with an image modification in the $L^*a^*b^*$ colour space and colour vectors and CIE94 difference equation are employed to estimate the gradient. Our future research will be focused on a better validation, with an extense dataset, on one hand, and, on the other hand, on segmenting the cup to estimate the CDR.

References

[1] S.Kavitha, S.Karthikeyan, K.Duraiswamy, Early Detection of Glaucoma in Retinal Images Using Cup to Disc Ratio, Proc. Int. Conf. on Computing, Communication and Networking Technologies(2010).

[2] Aliaa Abdel-Haleim Abdel-Razik Youssif, Atef Zaki Ghalwash, and Amr Ahmed Sabry Abdel-Rahman Ghoneim, Optic Disc Detection From Normalized Digital Fundus Images by Means of a Vessels Direction Matched Filter, IEEE Trans. on Medical Imaging, 27, 1 (2008).

[3] L. Gagnon, M. Lalonde, M. Beaulieu, and M.-C. Boucher, Procedure to detect anatomical structures in optical fundus images, Proc. Conf. Med. Imag. 2001, pp. 12181225. (2001).

[4] R. A. Abdel-Ghafar, T. Morris, T. Ritchings, and I. Wood, Detection and characterisation of the optic disk in glaucoma and diabetic retinopathy, Proc. Med. Image Understand. Anal. Conf. (1998).

[5] A. Osareh, M. Mirmehdi, B. Thomas, and R. Markham, Classification and localisation of diabetic-related eye disease, Proc. ECCV, May 2002, LNCS 2353, pp. 502516. (2002).

[6] Shijian Lu, Joo Hwee Lim,Automatic Optic Disc Detection From Retinal Images by a Line Operator, IEEE Trans. Biomedical Engineering, 58, 1 (2011).

[7] Ahmed E. Mahfouz, Ahmed S. Fahmy, Fast Localization of the Optic Disc Using Projection of Image Features, IEEE Trans. Image Processing, 19, 12 (2010).

[8] Arturo Aquino, Manuel Emilio Gegndez-Arias, Diego Marn, Detecting the Optic Disc Boundary in Digital Fundus Images Using Morphological, Edge Detection, and Feature Extraction Techniques, IEEE Trans. Medical Imaging, 29, 11 (2010).

[9] Fairchild, M.D., Color Appearance Models, (Wiley-IS&T) 2005, pg. 82.

[10] Abbas, Q., Celebi, M.E., Garca, I.F., Hair removal methods: A comparative study for dermoscopy images, Biomedical Signal Processing and Control 6 (4), pp. 395-404, (2011).

[11] Abbas Q., Fondon I., Rashid M., Unsupervised skin lesions border detection via two-dimensional image analysis, Comput. Meth. Prog. Bio. (2010).

[12] Bornemann F., Mrz T., Fast image inpainting based on coherence transport, J.Math. Imaging Vis. 28 (2007) 259?278.

[13] Muramatsu, C., Nakagawa, T., Sawada, A., Hatanaka, Y., Hara, T., Yamamoto, T., Fujita, H., Automated segmentation of optic disc region on retinal fundus photographs: Comparison of contour modeling and pixel classification methods, Computer Methods and Programs in Biomedicine 101 (1), pp. 23-32 (2010).

[14] Wong, D.W.K., Liu, J., Lim, J.H., Jia, X., Yin, F., Li, H., Wong, T.Y. Level-set based automatic cup-to-disc ratio determination using retinal fundus images in ARGALI. Conference proceedings : Annual International Conference of the IEEE Engineering in Medicine and Biology Society. IEEE Engineering in Medicine and Biology Society. pp. 2266-2269, (2008).

[15] Sáez, A., Serrano, C., Acha, B., Evaluation perceptual colour edge detection algorithms, 5th European Conference on Colour in Graphics, Imaging, and Vision and 12th International Symposium on Multispectral Colour Science 2010, CGIV 2010/MCS'10 , pp. 222-227 (2010).

[16] Plataniotis K.N., Venetsanopoulos A.N., Color Image Processing and Applications, Springer-Verlag, Berlin, 2000.

[17] Osher S. , Sethian J. A., Fronts propagating with curvaturedependent speed - algorithms based on hamilton-jacobi formulations, J

Comput Phys, 79, 12-49 (1998).

[18] Han X., Xu C., Prince J., A topology preserving level set method for geometric deformable models, IEEE Trans. Patt. Anal. Mach. Intell., vol. 25, pp. 755-768, (2003).

[19] Caselles V., Catte F., Coll T., Dibos F., A geometric model for active contours in image processing, Numer. Math., vol. 66, pp. 1-31, (1993).

[20] Malladi R., Sethian J. A., Vemuri B. C., Shape modeling with front propagation: a level set approach, IEEE Trans. Patt. Anal. Mach. Intell., vol. 17, pp. 158-175, (1995).

[21] C. Li, C. Xu, C. Gui, M. D. Fox, Level set evolution without re-initialization: a new variational formulation, IEEE Computer Society Conference on Computer Vision and Pattern Recognition, (2005).

[22] Fitzgibbon, A., Pilu, M., Fisher, R.B., Direct least square fitting of ellipses, IEEE Trans. Pattern Anal. Mach. Intell. 21 (5), pp. 476-480 (1999).

[23] Zhang, Z., Liu, J., Wong, W.K., Tan, N.M., Lim, J.H., Lu, S., Li, H., Wong, T.Y., Neuro-retinal optic cup detection in glaucoma diagnosis, Proceedings of the 2009 2nd Intern. Conf. on Biomedical Engineering and Informatics, BMEI 2009 , art. no. 5305076 (2009).

[24] Chrstek, R., Wolf, M., Donath, K., Niemann, H., Paulus, D., Hothorn, T., Lausen, B., Lammer, R., Mardin, C.Y., G., Michelson: Automated segmentation of the optic nerve head for diagnosis of glaucoma, Medical Image Analysis, 2005, 9 (4 SPEC. ISS.), pp. 297-314

[25] Xu, J., Chutatape, O., Chew, P., Automated optic disk boundary detection by modified active contour model, IEEE Trans. Biomed. Eng. 54 (3), art. no. 16, pp. 473-482 (2007).